Flight dynamics of a pterosaur-inspired aircraft utilizing a variable-placement vertical tail

Flight dynamics of a pterosaur-inspired aircraft utilizing a variable-placement vertical tail

Brian Roberts[1], Rick Lind[1] and Sankar Chatterjee[2]

[1] Department of Mechanical and Aerospace Engineering, University of Florida, Gainesville, FL 32611, USA
[2] Department of Geology and Paleontology Museum, Texas Tech University, Lubbock, TX 79409, USA

E-mail: ricklind@ufl.edu

Abstract
Mission performance for small aircraft is often dependent on the turn radius. Various biologically inspired concepts have demonstrated that performance can be improved by morphing the wings in a manner similar to birds and bats; however, the morphing of the vertical tail has received less attention since neither birds nor bats have an appreciable vertical tail. This paper investigates a design that incorporates the morphing of the vertical tail based on the cranial crest of a pterosaur. The aerodynamics demonstrate a reduction in the turn radius of 14% when placing the tail over the nose in comparison to a traditional aft-placed vertical tail. The flight dynamics associated with this configuration has unique characteristics such as a Dutch-roll mode with excessive roll motion and a skid divergence that replaces the roll convergence.

(Some figures in this article are in colour only in the electronic version)

1. Introduction

Turning is a critical metric when evaluating performance of many aircraft. In particular, micro air vehicles (MAVs) rely on turning for mission performance. Such vehicles are tasked with operating in urban environments for sensor emplacement in the presence of obstacles. An ability to reduce the radius of turns for these aircraft is clearly enhancing their mission effectiveness and performance.

The design community is rapidly adopting biologically inspired concepts as a valuable paradigm to enhance mission capability. The general concept notes that biological systems are often able to perform maneuvers that cannot be duplicated by engineered systems based on traditional designs; consequently, the aspects associated with that capability for biological systems can be incorporated into the engineered systems. Natural systems are used to inspire engineered systems in their modes of locomotion, maneuvers, and control systems [1–4]. In flight especially, both marine and aerial biological systems inspire vehicle configuration studies [5, 6].

The chemical processes used in nature, such as energy and reproduction, are being studied but remain challenging [7, 8]; however, the issues of shape changing and mass distribution through morphing that is used in nature are often realizable in aircraft using off-the-shelf technology.

A set of MAVs are developed and flown that directly incorporate biologically inspired morphing through articulated wings with shoulder and elbow joints along with twisting. One design rotates the wings vertically to mimic the variations in geometric dihedral displayed by seagulls to alter their gliding performance [9]. That design is extended to allow rotation that varies sweep of each joint to mimic a seagull flying with large crosswind [10]. Another design mimics the simultaneous variations in sweep and dihedral used by bats to initiate landing onto a vertical surface [11]. In each case, the designs are limited to concepts inspired by birds and bats along with being restricted to geometric modifications of the wings. Additional studies on other types of aircraft use passive and active morphing in the form of membrane wings [12], avian-inspired flaps [13], and springs for power reduction [14].
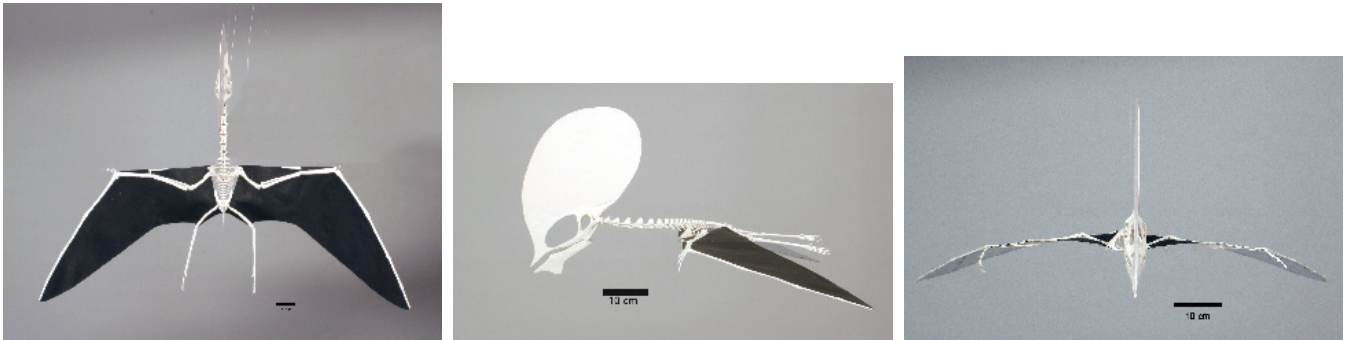
Figure 1. Skeletal reconstruction of pterosaur: dorsal view (left), lateral view (center) and anterior view (right).

This paper introduces a biologically inspired concept from pterosaurs to enhance mission performance; specifically, an aircraft is designed that incorporates a variable-placement vertical tail which is similar in nature to the cranial crest of the pterosaur [15]. This design allows the vertical tail to move aft in a traditional airplane configuration and move forward in a pterosaur-inspired configuration. The flight dynamics are analyzed using computational aerodynamics to observe the variations in static stability and unique modes that evolve. Finally, moving the vertical tail over the nose is shown to have an adverse effect on both static and dynamic stability but can reduce the turn radius by 14%.

2. Biological inspiration

2.1. Pterosaur

The only tetrapods that currently are capable of powered flight are birds and bats; however, pterosaurs were actually the first vertebrates to achieve flight which occurred about 225 000 000 years ago [15]. They first appeared in the fossil record during the late Triassic and diversified into an extraordinary variety of forms and sizes during the Jurassic and Cretaceous periods. They then continued to dominate the sky throughout the Mesozoic period until they became extinct at the end of the Cretaceous period, about 65 000 000 years ago, along with the dinosaurs. As such, the species survived for about 160 000 000 years.

Pterosaurs have a unique wing anatomy that differs noticeably from birds and bats. The wings of a pterosaur consist of a thin membrane which is supported by forelimbs and a hyper-elongated fourth finger that comprises over half of the span. This wing membrane is partitioned into four panels stretched between the skeletal structure of the wing and the hindlimbs. There is controversy amongst the paleontological community as to whether or not the hindlimbs played a role in lift production and flight control [16, 17]. Also, the wing membrane is semi-rigid due to reinforcement from parallel fibers of actinofibrils. These fibers are oriented perpendicular to the direction of span-wise tension to maximize strength and stiffness during flight [18]. They even fold together to reduce the wing area when walking.

A range of sizes are observed in pterosaurs over the span of their evolution with mass ranging from 0.012 to 70 kg and

Table 1. Ranges of parameters for pterosaurs.

Parameter	Pterosaur
Wingspan (m)	[0.3, 10.40]
Mass (g)	[12, 70 000]
Mode	Hover, cruise, soar
Environment	Gusty, cluttered

wingspan ranging from 0.4 to 10.1 m. Actually, the species of *Quetzalcoatlas* became the largest animal to achieve self-powered flight. The flight performance of many species of pterosaurs was studied and correlated size with estimated flight capabilities; namely small-sized pterosaurs with mass between 0.01 and 0.2 kg were likely capable of hovering flight, medium-sized pterosaurs with mass between 0.3 and 9.0 kg were likely capable of powered flight, and large-sized pterosaurs with mass between 9.0 and 70.0 kg were likely restricted to soaring flight [15].

This paper specifically considers a skeleton of a *Tapejara wellnhoferi* to obtain estimates of limb motion and mass properties. This skeleton, as shown in figure 1, was recovered in Brazil from a pterosaur that lived in the early Cretaceous period about 125 000 000 years ago. The estimated mass of the pterosaur was 0.4 kg with a wingspan of 1.4 m.

2.2. Suitability

Pterosaurs are remarkably suitable for biologically inspired design of aircraft. The community has invested considerable effort into the study of birds and insects for design; however, pterosaurs are actually very appropriate for a variety of specific well-defined reasons.

(1) The range of specimen size for pterosaurs is relatively large and appropriate for missions ranging from high-altitude environments to urban environments. Some characteristics, as shown in table 1, are shown to vary with dimensions covering these classes of aircraft. As such, designs based on these concepts can utilize the scalability already demonstrated by nature for the aerodynamics to expand the mission capability.

(2) Pterosaurs are of particular interest due to the ability to both walk on the ground and sail over water in addition to flight. Such multi-modal locomotion enables an incalculable range of missions. An aircraft based on
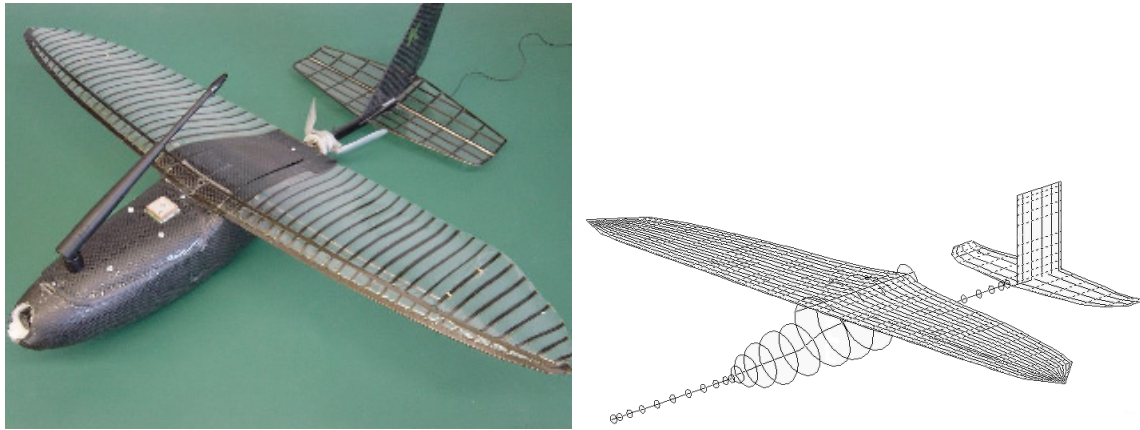
Figure 2. Existing aircraft (left) and baseline shape for pterosaur-inspired vehicle (right).

Table 2. Properties of flight platforms.

Platform	Wing surface	Muscle actuation	Flapping motion	Vertical tail	Wing extension	Structural elements
Insect	Rigid	Low	High	No	No	Chord-span
Bird	Feather	Low	High	No	Feathers	Span
Bat	Membrane	High	High	No	Joints [21]	Chord-span
Pterosaur	Membrane	Low	Low	Yes	Joints	Span
MAV	Membrane	Low	Low	Yes	Joints	Span

pterosaur concepts may be able to fly to a rooftop, and then walk under an overhang to mount a sensor in a dark corner.

(3) Also, the choice of pterosaur for biological inspiration is actually quite appropriate as compared to other species in nature when considering mechanical requirements. Certainly the community has had success looking to birds and bats; however, pterosaur characteristics are best aligned with those of existing MAV types that have been successfully flown by the research team as shown in table 2. Additionally, the pterosaur flight apparatus has been concluded to have been ideal for slower flight speeds, being both highly efficient and highly maneuverable [19, 20].

3. Platform design

3.1. Baseline shape

A vehicle is designed that incorporates some characteristics inspired by a pterosaur. A baseline shape is chosen from an existing vehicle with dimensions similar to those of a small pterosaur. The computational model of the baseline vehicle is shown along with the existing aircraft in figure 2.

The specific parameters of the vehicle are given in table 3.

The model has a total weight of 611 g. This mass is distributed as 295 g for the fuselage, 90 g for the wings, 15 g for the tailboom, 15 g for the noseboom, 8 g for the horizontal tail, and 8 g for the vertical tail. Additional avionics consist of a battery near the center of the fuselage weighing 130 g and a motor near the aft of the fuselage weighting 50 g.

Table 3. Characteristics of the baseline vehicle.

Parameter	Value
Wingspan	80.3 cm
Wing area	945.16 cm^2
Reference chord	11.94 cm
Center of gravity	[−1.27, 0.0, −3.17] cm
Vertical tail area	83.87 cm^2
Vertical tail chord length	7.36 cm
Vertical tail span	11.43 cm
Horizontal tail area	189.68 cm^2
Horizontal tail chord length	8.38 cm
Horizontal tail span	29.21 cm
Fuselage length	29.46 cm
Fuselage width	9.65 cm

A set of control effectors are elevator and aileron along with rudder. The elevator is defined, chordwise, as the aft 57% of the horizontal tail along its entire span. The ailerons are defined, chordwise, as the aft 50% of the wing along the outermost 40% of the wingspan. The rudder is defined as the entire vertical tail surface which can rotate about the leading-edge axis.

3.2. Vertical tail

A critical feature of the pterosaur is the cranial crest which has obvious similarities, except for the position, to the vertical tail on an aircraft. This cranial crest is actually on the head so it can move up or down as the neck is moved; consequently, the vertical tail on this aircraft is allowed to translate longitudinally along the fuselage and translate vertically through the fuselage as shown in figure 3.
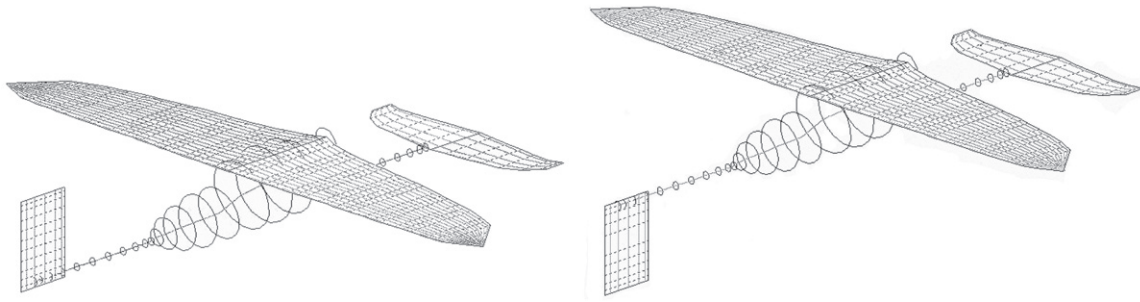
Figure 3. Configurations with a vertical tail at the nose.
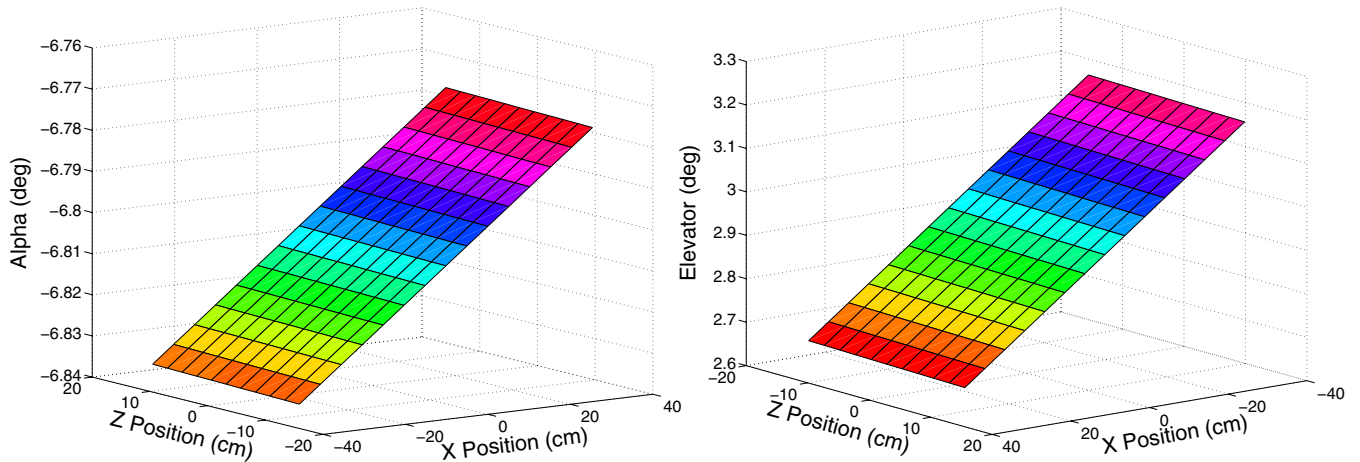

Figure 4. Trim for straight-and-level flight: angle of attack (left) and elevator deflection (right).

The vertical tail is allowed to range across the entire fuselage. As such, the position of this element varies from 35.5 cm forward to 35.5 cm aft of the center of gravity along with 12.7 cm above to 12.7 cm below the center of gravity. It is also allowed to rotate about the leading-edge axis by 45° in either direction.

3.3. Platform analysis

The flight dynamics are analyzed using Athena Vortex Lattice (AVL) to estimate the aerodynamics [22]. This low-order code makes assumptions that the flow is incompressible and inviscid; however, it is widely used in the community and predicts aerodynamics that have been shown in certain cases to have specific values within 20% of experimental measurements for this class of MAVs thin wings [23–32]. The aerodynamics of the wings are estimated along with the flow associated with slender bodies such as the fuselage.

AVL assumes quasi-steady flow so unsteady vorticity shedding is neglected. More precisely, it assumes the limit of small reduced frequency which means that any oscillatory motion must be slow enough so that the period of oscillation is much longer than the time it takes the flow to traverse an airfoil chord. This assumption is virtually valid for any expected flight maneuver of the vehicle. Also, the rates in roll, pitch and yaw used in the computations must be slow enough so that the resulting relative flow angles are small as judged by the dimensionless rotation rate parameters.

4. Static stability

4.1. Straight and level flight

4.1.1. Trim. A set of trim conditions are identified for the model having steady straight-and-level flight at 24 m s^{-1}. The conditions are found by varying the control surfaces to balance the forces and moments. Also, the angle of attack is constrained to provide the required lift while the angle of sideslip is constrained to zero.

The variations of the longitudinal parameters, such as angle of attack and elevator along with the lift-to-drag ratio, associated with trim are shown in figure 4. These parameters increase as the vertical tail is moved forward toward the nose; however, they remain relatively unchanged in the presence of variations in the vertical position of the tail. The forward translation of the vertical tail creates a small change in the center of gravity which causes these small variations in trim parameters. The elevator must deflect less as the tail, and associated center of gravity, moves forward because it generates a larger moment; similarly, the decrease in elevator is accompanied by a loss of lift so the angle of attack must then increase to replace that lost lift.

4.1.2. Stability derivatives. The vehicle remains statically stable about the lateral axis for any position of the vertical tail. The condition for stability is a negative value for the coefficient of pitch moment due to the angle of attack, denoted
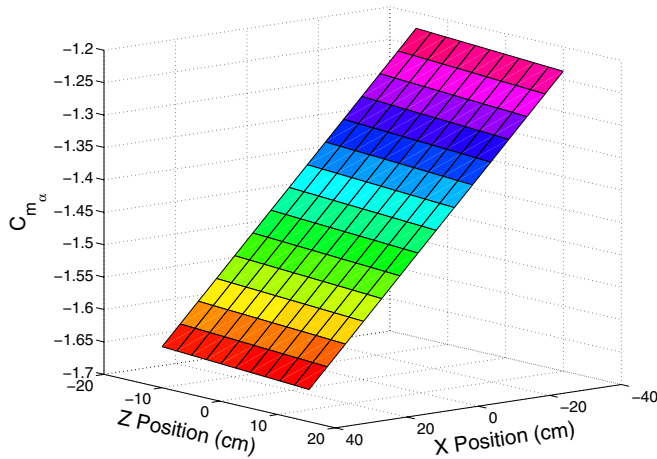
4

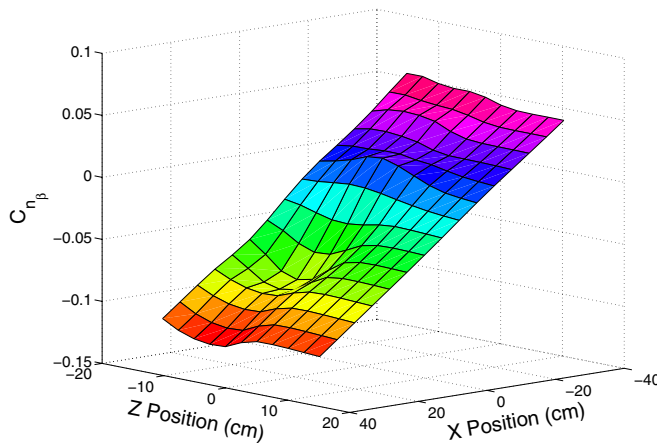**Figure 5.** Pitch moment coefficient with respect to the angle of attack for straight-and-level flight.

Figure 6. Yaw moment coefficient with respect to the angle of sideslip for straight-and-level flight.

as C_{m_α}, which is shown for all configurations in figure 5. The actual value has small variation with longitudinal position and negligible variation with vertical position. This lack of significant variation agrees with the predominately lateral–directional nature of the vertical tail as a control effector.

The static stability about the vertical axis shows negligible variation in vertical position and increasing variation in longitudinal position. Similar trends are shown for the lateral axis in figure 6; however, the trends actually result in some configurations being statically unstable about the vertical axis. The condition for static stability, which requires C_{n_β} as the coefficient of yaw moment with respect to the angle of sideslip to be positive, is only satisfied when the vertical tail is aft of the center of gravity. The variation due to longitudinal position results directly from an increase in the moment arm and thus has a similar effect on static stability as elevator deflection at trim as shown in figure 4.

The static stability about the longitudinal axis, unlike either the lateral or vertical axes, displays noticeable variation due to changes in both the longitudinal position and vertical position of the vertical tail. This static stability is determined
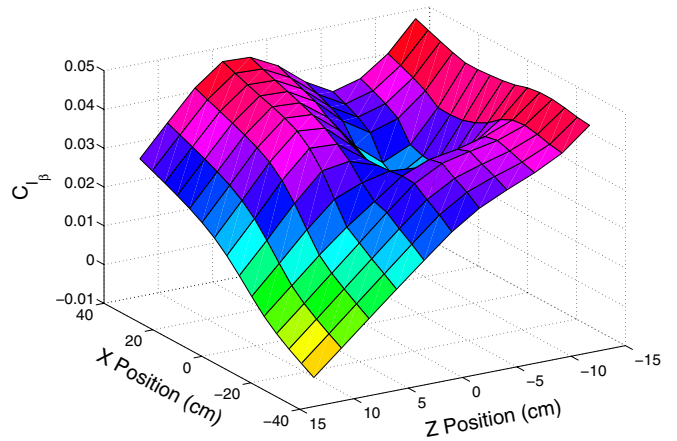

Figure 7. Roll moment coefficient with respect to the angle of sideslip for straight-and-level flight.

by a negative value for the coefficient of roll moment due to the angle of sideslip, denoted as C_{l_β}, and is shown in figure 7. The basic trends show that the coefficient increases as the vertical tail is moved down and forward; however, some unexpected behavior is observed as the coefficient decreases in a small region of positions surrounding the origin. As such, a configuration with the vertical tail placed forward and above the center of gravity is the only configuration with static stability about the longitudinal axis.

4.2. Banked turning flight

4.2.1. Trim. A set of trim conditions are identified for the model during a banked turn with a roll angle of $45°$ and a $1.41 - g$ loading when considering the vertical tail at various longitudinal positions and deflection angles. The deflections of the control surfaces that balance the forces and moments to maintain this flight condition are computed. Also, the angle of attack and angle of sideslip are allowed to vary to maintain constant lift equal to the vehicle weight and counteract any moments produced by the vertical tail. The flight condition will consider speeds at which 2 N of drag is maintained. This constant drag assumption stems from the fact that jet engines exhibit constant thrust at all flight speeds, and the value of assumed thrust for the aircraft is chosen arbitrarily. Propeller motors exhibit constant power across flight speeds. Tests that make an assumption of constant power show very similar results to the data shown in this paper, and thus are not shown to avoid redundancy.

The variations in the longitudinal parameters associated with the angle of attack and elevator deflection are shown in figure 8. The dominant trend is an increase in the angle of attack as the deflection of the vertical tail increases. This increase in the angle of attack results from an increase in drag as the vertical tail deflects. Also, the elevator decreases its deflection as the deflection of the vertical tail increases.

The lateral–directional parameters required for trim are shown in figure 9 for the angle of sideslip and aileron deflection. The aileron deflection required to trim does
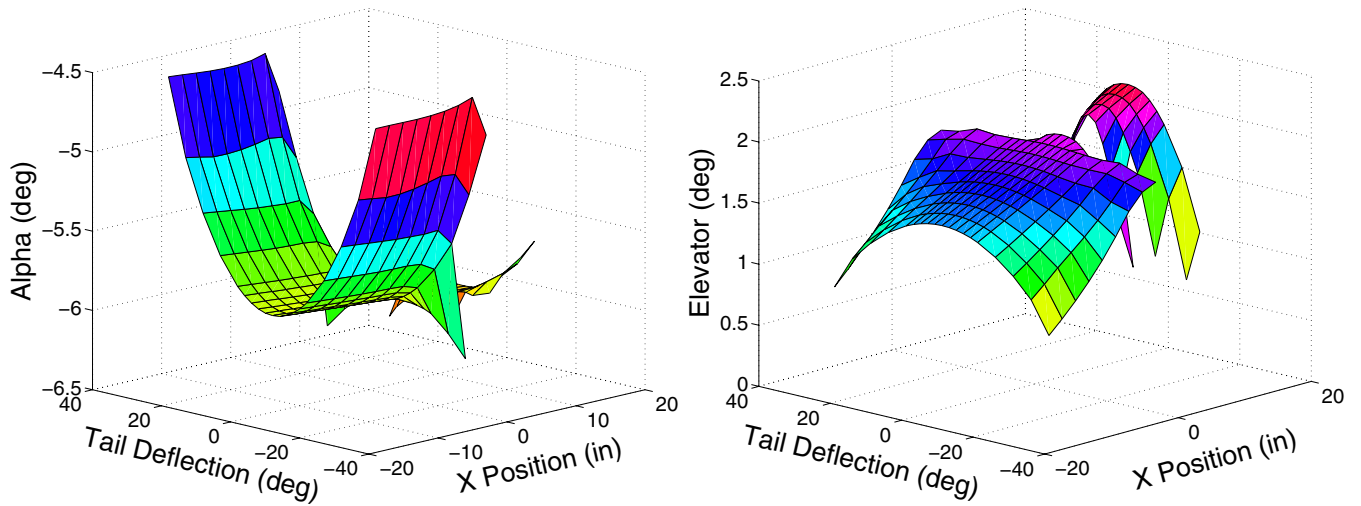
5

Figure 8. Trim in a 45° banked turn: angle of attack (left) and elevator deflection (right).
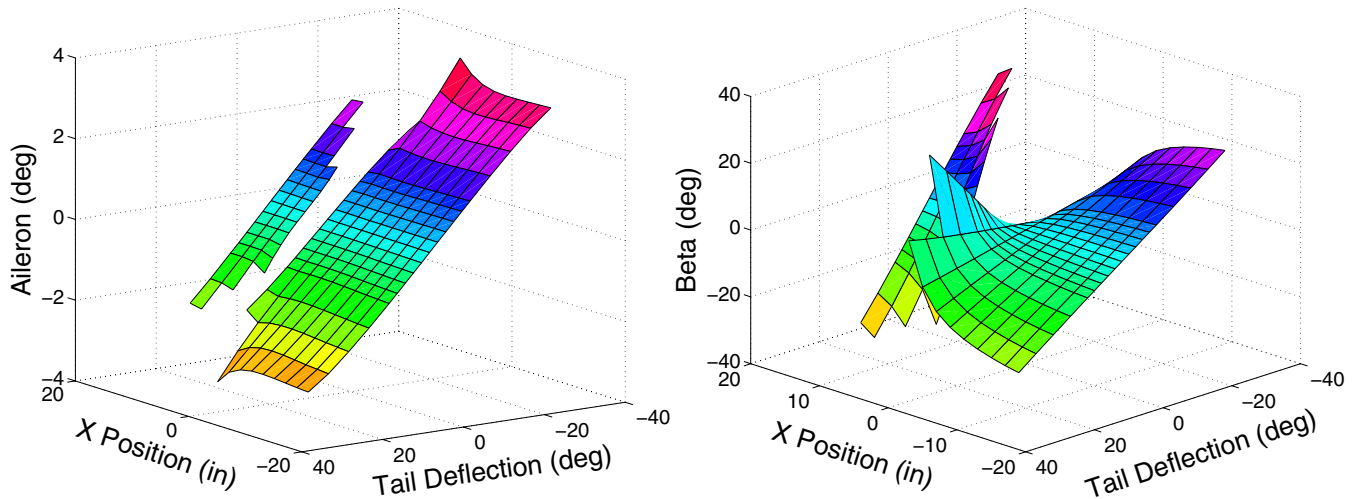

Figure 9. Aileron deflection and angle of sideslip in a 45° banked turn.

not vary with the position of the vertical tail; however, it decreases as increasing deflection of the vertical tail induces a roll moment that must be countered from the aileron. The angle of sideslip is also varied because of the yaw moment produced by a non-zero deflection of the vertical tail. This variation matches the tail deflection in magnitude and alternates directions for the vertical tail being located forward or aft of the center of gravity.

4.2.2. Stability derivatives. The coefficient of pitching moment with respect to the angle of attack, as shown in figure 10, exhibits a parabolic trend as the vertical tail deflects at about 0°. The coefficient also shows some variation with longitudinal position such that it becomes more negative as the tail is moved further aft.

The coefficient of yaw moment with respect to the angle of sideslip as shown in figure 11 is nearly constant for variations in deflection of the vertical tail but shows a linear relationship to variations in the longitudinal position. Such a relationship relates to variations in the moment arm as the vertical tail
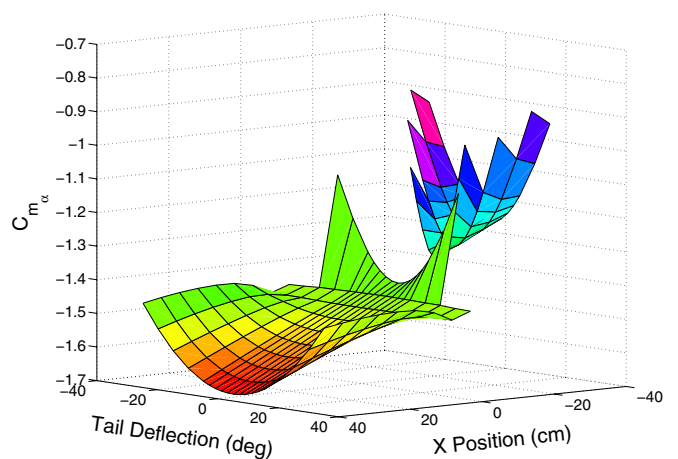

Figure 10. Pitch moment coefficient with respect to the angle of attack in a 45° banked turn.

and its associated sideforce move relative to the center of gravity. The vehicle has static stability in the directional axis
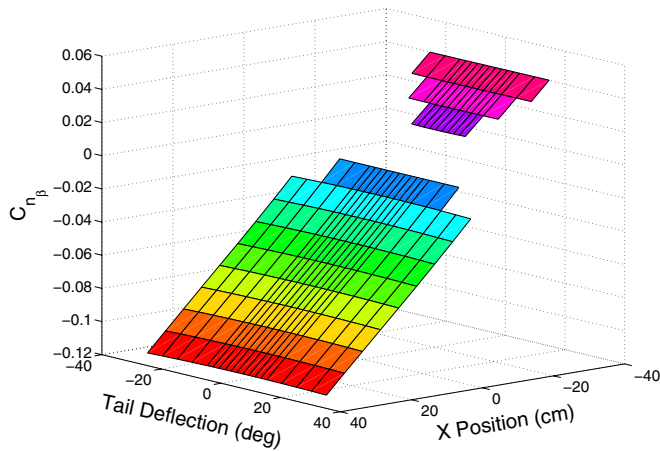
Figure 11. Yaw moment coefficient with respect to the angle of sideslip in a 45° banked turn.

Figure 12. Roll moment coefficient with respect to the angle of sideslip in a 45° banked turn.

for configurations with a vertical tail being far behind the center of gravity.

The coefficient of roll moment with respect to a sideslip angle, shown in figure 12, shows distinct trends with respect to both longitudinal position and deflection of the vertical tail. This stability derivative increases in a nearly-linear fashion as the vertical tail is moved forward and, except for a discontinuity around small negative deflection angles, exhibits a nearly inverse-parabolic shape with respect to deflection angles. The inverse parabola from the latter trend is centered about a deflection angle of zero such that the largest values of C_{l_β} result from the smallest deflections. As such, the vehicle has static stability about the longitudinal axis only for large deflections of the vertical tail when forward of the center of gravity, but is stable for any deflections as the vertical tail is located aft of the center of gravity.

4.2.3. Turn radius. The characteristics of the turn resulting from these trim conditions are shown in figure 13 for both turn radius and turn rate. The turn radius is clearly reduced as the vertical tail is deflected and moved forward along the fuselage.
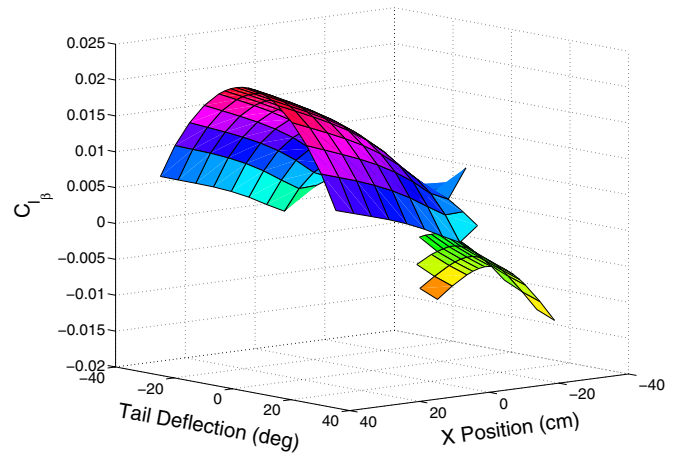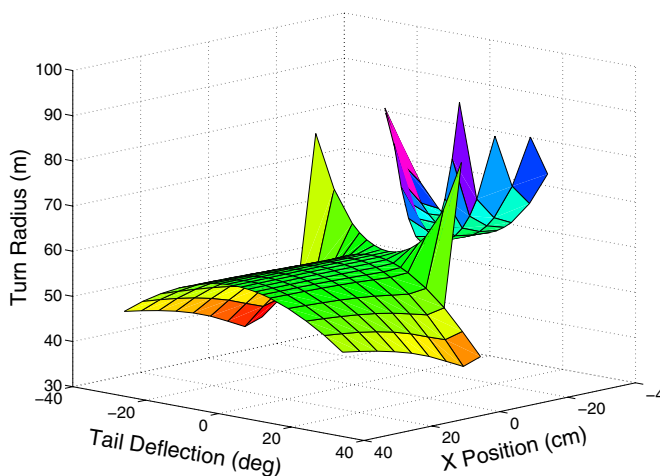
Table 4. Turn radius in m at extremal values of position and angle for the vertical tail.

	Angle of −25°	Angle of 0°	Angle of +25°
Rear placement ($x = -35.56$ cm)	84.43 m	58.02 m	84.05 m
Forward placement ($x = +35.56$ cm)	50.40 m	57.65 m	50.31 m

This reduction in the turn radius is accompanied by the related increase in the turn rate.

The values of the turn radius are extracted from figure 13 at configurations with the largest values of position and angle for the vertical tail. These values, as given in table 4, clearly demonstrate that placing the vertical tail over the nose has a lower radius and thus greater agility as compared to placing the vertical tail in the rear.

The reduction in the turn radius is caused by an increase in the drag coefficient that decreases the velocity at which drag is 2 N as shown in figure 14.

The increase in turn performance is directly a result of the flight properties at trim shown in figure 14 which in turn
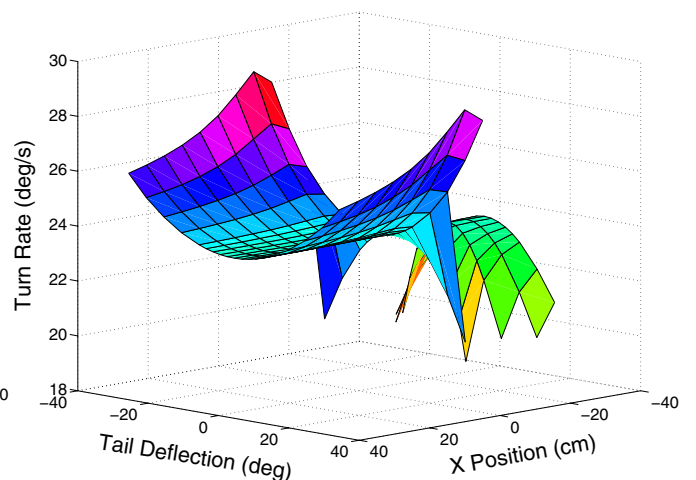

Figure 13. Turning metrics in a 45° banked turn with respect to vertical tail deflection and longitudinal placement.
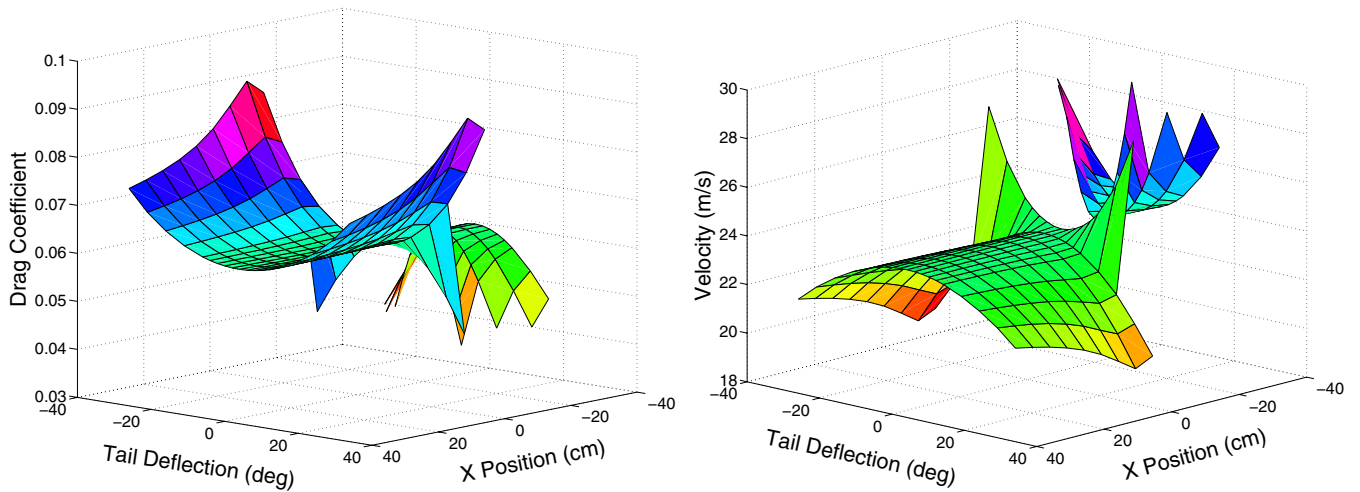
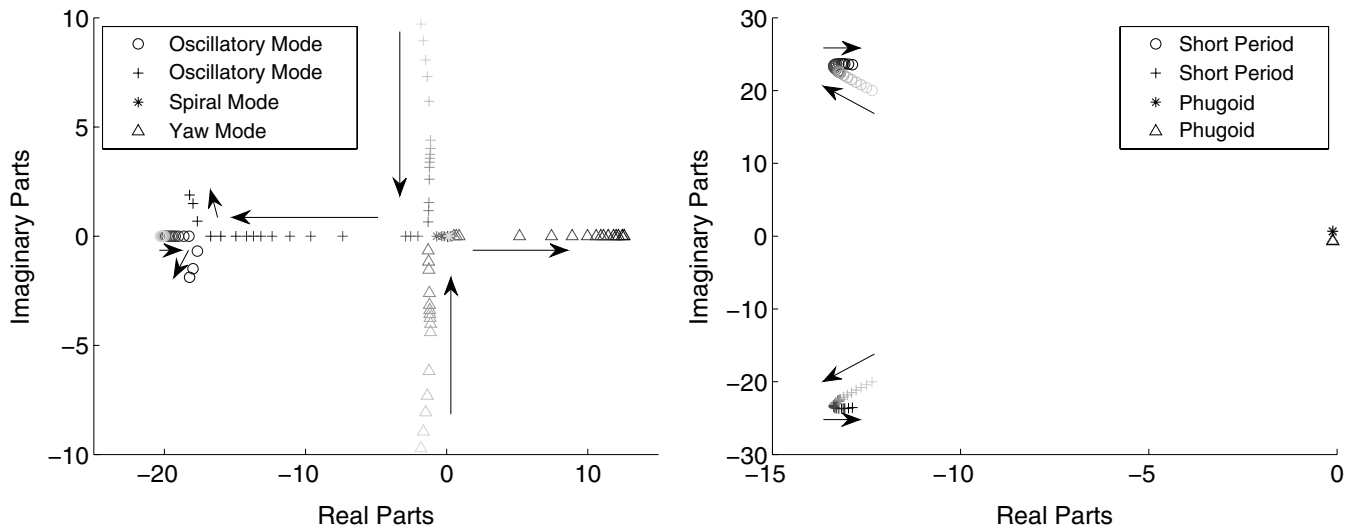**Figure 14.** Drag coefficient and trim velocity in a 45° banked turn.

Figure 15. Eigenvalues as the vertical tail moves forward: lateral–directional (left) and longitudinal (right).

result from the aircraft parameters shown in figure 9; however, the fundamental cause is actually the relationship between the center of gravity and the vertical tail. In this case, the aircraft is trim for a turn with the nose rotating to the right. The aft placement of the tail requires a positive angle of sideslip to trim while the forward placement requires a negative angle of sideslip. These conditions imply that the aft placement requires the nose of the aircraft to point away from the direction of turn while the forward placement requires the nose to point into the direction of turn. As such, moving the vertical tail forward means the aerodynamic center, at which its sideforce can be represented, is in front of the center of gravity so the aircraft trim, and thus its drag, is significantly different.

5. Flight dynamics

5.1. Straight-and-level flight

5.1.1. Trim. The flight dynamics are analyzed for the pterosaur-inspired aircraft when trim is in the straight-and-level condition. This analysis indicates that the flight

dynamics are dramatically more sensitive to variations of the longitudinal position than the vertical position of the vertical tail; consequently, results are discussed only for the vehicle with a vertical tail positioned to have its aerodynamic center located 2.6 cm above the center of mass of the aircraft while the longitudinal position is varied.

5.1.2. Eigenvalue analysis. The eigenvalues associated with the flight dynamics are shown in figure 15 to vary as the vertical tail is moved along the longitudinal axis. The eigenvalues associated with the longitudinal dynamics show minor variation for the phugiod mode and negligible variation for the short-period mode; however, the eigenvalues associated with the lateral–directional dynamics vary quite significantly for all the modes. The complex-conjugate pair of poles associated with the Dutch-roll mode when the tail is placed at the rear actually converge as the tail moves forward and become a pair of real poles. One pole remains real while the other pole couples with the original roll convergence to form a new complex-conjugate pair. The break-away point
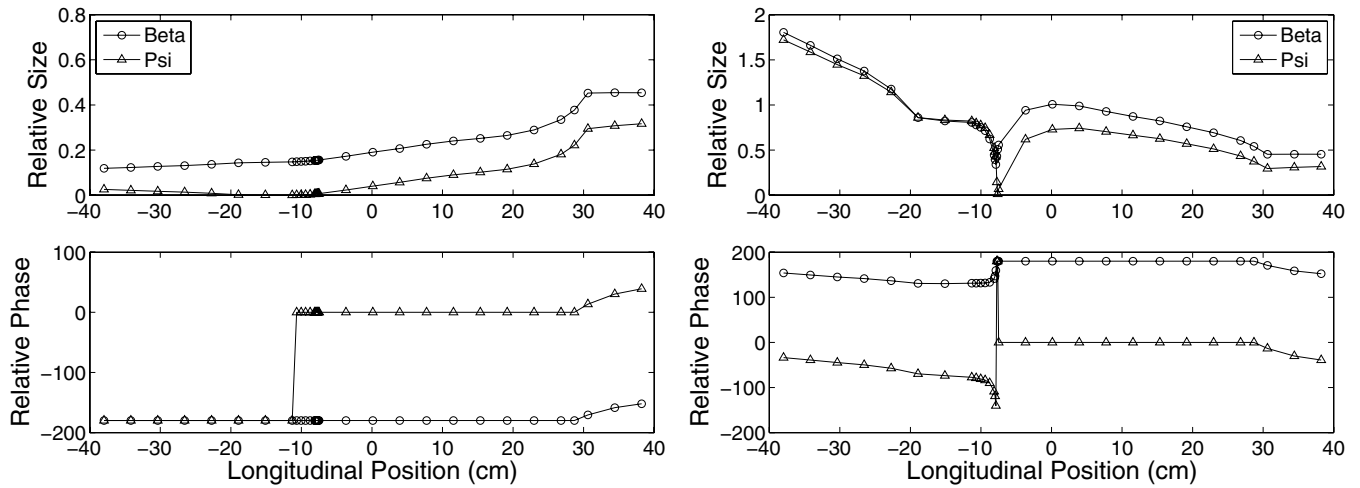
Figure 16. Eigenvectors for variations in the longitudinal location of the vertical tail for eigenvalue associated with aft-location roll convergence (left) and aft-location Dutch-roll mode (right) with a normalized roll angle.

for this behavior involving the Dutch-roll mode is a vertical tail at a value of 5.3 cm behind the center of gravity whereas the break-in point for coupling with the roll convergence is a vertical tail at a value of 30.2 cm in front of the center of gravity.

The stability of the flight dynamics is directly evident by the eigenvalues of figure 15 for variations in the vertical tail. The longitudinal dynamics remain stable for any location of the vertical tail while the lateral–directional dynamics remain unstable. The vehicle has a single unstable pole for aft locations of the vertical tail but has a pair of unstable poles, both real, for locations of the vertical tail that are forward of the center of gravity.

5.1.3. Eigenvector analysis. The eigenvectors are analyzed to determine the mode shapes of the flight dynamics. Such information is presented as the magnitude of states relative to a normalized state. In this case, only the eigenvectors

of the lateral–directional dynamics are presented since the longitudinal modes do not vary significantly.

The eigenvectors are shown in figure 16 that are associated with eigenvalues which couple to generate a new oscillatory mode. When the vertical tail is at the rear, these eigenvectors indicate that one motion is characterized by the roll angle being 20 times the value of the yaw angle and another motion is characterized by nearly equal but opposite values for the yaw angle and angle of sideslip with the roll angle being half their value. As such, the eigenvalues relate a roll convergence and the Dutch-roll mode for this traditional aft-location configuration. The forward movement of the vertical tail causes a coupling of the pair of eigenvalues with the new mode having a yaw angle slightly smaller but still opposite in sign to the angle of sideslip while the roll angle is about twice their value. As such, the new mode closely resembles a Dutch-roll mode but with more roll than would normally be associated with such a mode. The characteristics of this new mode are somewhat expected given that the dynamic associated with
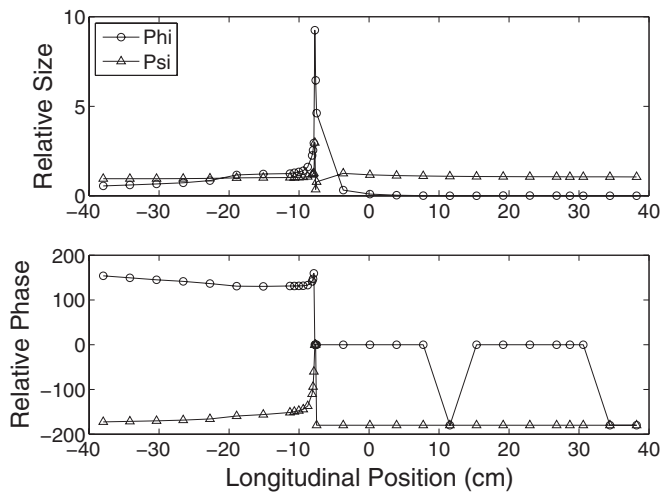

Figure 17. Eigenvectors for variations in the longitudinal location of the vertical tail for eigenvalue associated with aft-location Dutch-roll mode with a normalized angle of sideslip.
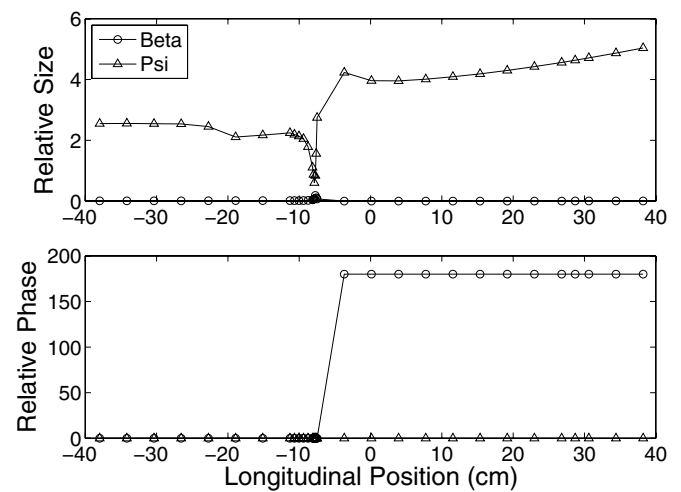

Figure 18. Eigenvectors for variations in the longitudinal location of the vertical tail for eigenvalue associated with aft-location spiral divergence with a normalized roll angle.
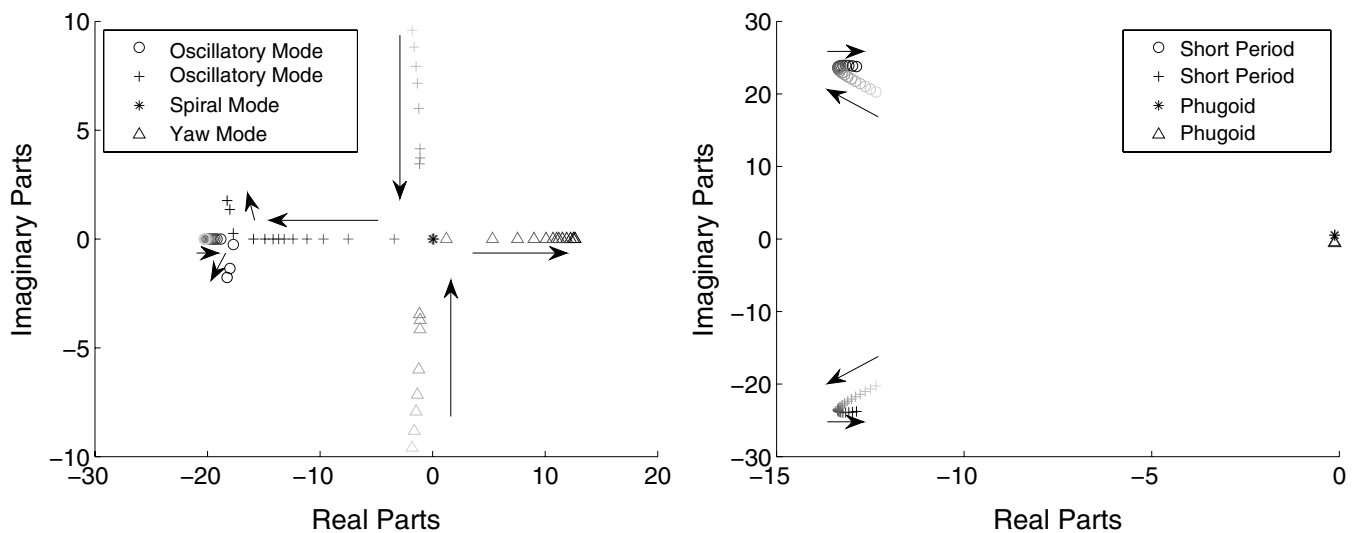
9

Figure 19. Turning mode eigenvalues as the vertical tail moves forward: lateral (left) and longitudinal (right).

nearly-pure roll motion are merged with a traditional Dutch-roll motion.

The eigenvector in figure 17 indicates the mode shape for the pole that transitions from a Dutch-roll mode to a skid divergence. The mode shape for the vertical tail at the rear shows oscillatory motion with the traditional relationship between states for a Dutch-roll mode such as equal but opposite yaw angle and angle of sideslip with the roll angle being half their size; however, the mode shape for the vertical tail at the front shows non-oscillatory motion of equal but opposite yaw angle and angle of sideslip with a negligible roll angle. Such a motion is visualized as a skidding motion, with the vehicle beginning to rotate as it continues to translate in the initial direction of travel. If left uncorrected by control effectors, the yaw motion will worsen until the vehicle enters a flat spin. This motion is somewhat expected given the lack of directional static stability indicated in figure 6 for forward locations of the vertical tail.

The remaining eigenvector in figure 18 shows the mode shape of the spiral divergence. The movement of the vertical tail from the rear to the front is characterized only by a small increase in relative magnitude for the yaw angle and a change in phase between the yaw angle and the roll angle. The yaw angle and roll have the same sign for the vertical tail in the rear but have opposite signs for the vertical tail in the front.

5.2. Turning modal analysis

The locus of eigenvalues are given in figure 19 as the vertical tail is moved during turning flight. These eigenvalues are nearly identical to those during straight-and-level flight. As such, the discussions of eigenvalues and eigenvectors are redundant to those of the straight-and-level flight.

6. Conclusion

The order of pterosaur survived for 160 000 000 years with a cranial crest that was inherently destabilizing; consequently, some advantage must have been realized for this instability

to have evolved. While some researchers believe that the advantage of the crest could have been for mating or even thermal diffusion, the large vertical surface must have had some aerodynamic impact. A model that incorporates a vertical tail that can range from a traditional aft placement to a pterosaur-inspired forward placement is used to analyze the crest's aerodynamic impact and its applicability to aircraft. The turn performance is clearly improved by placing the tail over the nose although such a configuration is accompanied by a corresponding loss of static and dynamic stability. This tradeoff between performance and stability can be varied by including a morphing capability that varies the location of the vertical tail during flight.

References

[1] Boria F J, Bachmann R J, Ifju P G, Quinn R D, Vaidyanathan R, Perry C and Wagener J 2005 A sensor platform capable of aerial and terrestrial locomotion IROS 2005: *Proc. IEEE/RSJ Int. Conf. Intelligent Robots and Systems* pp 3959–64

[2] Cory R and Tedrake R 2008 Experiments in fixed-wing UAV perching *AIAA Guidance, Navigation and Control Conf.* AIAA-2008-7256

[3] Franceschini N, Ruffier F and Serres J 2007 A bio-inspired flying robot sheds light on insect piloting abilities *Curr. Biol.* **17** 329–35

[4] Shim Y and Husbands P 2007 Feathered flyer: integrating morphological computation and sensory reflexes into a physically simulated flapping-wing robot for robust flight manoeuvre *Lecture Notes Comput. Sci.* **4648** 756–65

[5] Lazos B S 2005 Biologically inspired fixed-wing configuration studies *J. Aircr.* **42** 1089–98

[6] Davidson J B, Chwalowski P and Lazos B S 2003 Flight dynamic simulation assessment of a morphable hyper-elliptic cambered span winged configuration *AIAA Atmospheric Flight Mechanics Conf.* AIAA-2003-5301

[7] Shimizu K 2009 Toward systematic metabolic engineering based on the analysis of metabolic regulation by the integration of different levels of information *Biochem. Eng. J.* **46** 235–51

[8] Zykov V, Mytilianaios E, Adams B and Lipson H 2005 Self-reproducing machines *Nature* **435** 163

[9] Abdulrahim M and Lind R 2004 Flight testing and response characteristics of a variable Gull-wing morphing aircraft *AIAA Guidance, Navigation and Control Conf.* AIAA-2004-5113

[10] Grant D T, Abdulrahim M and Lind R 2006 Flight dynamics of a morphing aircraft utilizing independent multiple-joint wing sweep *AIAA Atmospheric Flight Mechanics Conf.* AIAA-2006-6505

[11] Grant K and Lind R 2009 Sensor emplacement on vertical surfaces with biologically-inspired morphing from bats *J. Aircr.* **46** 1450–4

[12] Song A, Tian X, Israeli E, Galvao R, Bishop K, Swartz S and Breuer K 2008 The aero-mechanics of low aspect ratio compliant membrane wings, with applications to animal flight *46th AIAA Aerospace Sciences Meeting and Exhibit* AIAA-2008-517

[13] Kernstine K H, Moore C J, Cutler A and Mittal R 2008 Initial characterization of self-activate movable flaps, 'Pop-up Feathers' *46th Aerospace Sciences Meeting (Reno, NV, 7–10 January 2008)* AIAA-2008-369

[14] Isaac K K and Agrawal S K 2007 An investigation into the use of springs and wing motions to minimize the power expended by a pigeon-sized mechanical bird for steady flight *J. Mech. Design* **129** 381–9

[15] Chatterjee S and Templin R J 2004 *Posture, Locomotion and Paleoecology of Pterosaurs* (*Geological Society of America Special Publication* vol 376) pp 1–64

[16] Unwin D M and Bakhurina N N 1994 Sordes pilosus and the nature of the pterosaur flight apparatus *Nature* **371** 62–4

[17] Padian K 1983 A functional analysis of flying and walking in pterosaurs *Paleobiology* **9** 218–39

[18] Bennett S C 2000 Pterosaur flight: the role of actinofibrils in wing function *Historical Biol.* **14** 255–84

[19] Stein R S 1975 Dynamic analysis of Pteranodon ingens: a reptilian adaptation to flight *J. Paleontology* **49** 534–48

[20] Hazlehurst G A and Rayner J M V 1992 Flight characteristics of Triassic and Jurassic Pterosauria: an appraisal based on wing shape *Paleobiology* **18** 447–63

[21] Prondvai E and Hone D W E 2008 New models for the wing extension in pterosaurs *Historical Biol.* **20** 237–54

[22] Drela M and Youngren H AVL—aerodynamic analysis, trim calculation, dynamic stability analysis, aircraft configuration development, Athena Vortex Lattice, v. 3.15 (available at http://raphael.mit.edu/avl/)

[23] Stanford B, Abdulrahim M, Lind R and Ifju P 2007 Investigation of membrane actuation for roll control of a micro air vehicle *J. Aircr.* **44** 741–9

[24] Traub L W 2009 Experimental investigation of annular wing aerodynamics *J. Aircr.* **46** 988–96

[25] Gopalarathnam A and Norris R K 2009 Ideal lift distributions and flap angles for adaptive wings *J. Aircr.* **46** 562–71

[26] Cox C, Gopalarathnam A and Hall C E 2009 Development of stable automated cruise flap for an aircraft with adaptive wing *J. Aircr.* **46** 301–11

[27] Boschetti P, Cardena E, Amerio A and Arevalo A 2010 Stability and performance of a light unmanned airplane in ground effect *AIAA Aerospace Sciences Meeting* AIAA-2010-293

[28] Leong H I, Jager R, Keshmiri S and Colgren R 2010 Development of a pilot training platform for UAVs using a 6DOF nonlinear model with flight test validation *AIAA Modeling and Simulation Conf.* AIAA-2008-6368

[29] Royer D A, Keshmiri S, Sweeten B C and Jones V 2010 Modeling and sensitivity analysis of the meridian unmanned aircraft *AIAA Infotech@Aerospace* AIAA-2010-3468

[30] Stewart K, Abate G and Evers J 2006 Flight mechanics and control issues for micro air vehicles *AIAA Atmospheric Flight Mechanics Conf.* AIAA-2006-6638

[31] Stewart K, Wagener J, Abate G and Salichon M 2007 Design of the air force research laboratory micro aerial vehicle research configuration *AIAA Aerospace Sciences Meeting* AIAA-2007-667

[32] Stewart K, Blackburn K, Wagener J, Czabaranek J and Abate G 2008 Development and initial flight tests of a single-jointed articulated-wing micro air vehicle *AIAA Atmospheric Flight Mechanics Conf.* AIAA-2008-6708